SEMARAK ILMU PUBLISHING

CFD Letters

Journal homepage:
https://semarakilmu.com.my/journals/index.php/CFD_Letters/index
ISSN: 2180-1363

Computational Elucidation of Electromagnetic Effects on Peristaltic Nanofluid Transport in Microfluidics: Intersections of CFD, Biomedical and Nanotechnology Research

Hanumesh Vaidya[1], Rajashekhar Choudhari[2], Fateh Mebarek-Oudina[3], Kerehalli Vinayaka Prasad[1], Manjunatha Gudekote[4], Balachandra Hadimani[4,*], Sangeeta Kalal[1], Shivaleela[1]

[1] Department of Mathematics, Vijayanagara Sri Krishnadevaraya University, Ballari, Karnataka, India
[2] Department of Mathematics, Manipal Institute of Technology, Bengaluru, Manipal Academy of Higher Education, Manipal, Karnataka, India
[3] Department of Physics, Faculty of Sciences, University of 20 août 1955-Skikda, Skikda 21000, Algeria
[4] Department of Mathematics, Manipal Institute of Technology, Manipal, Manipal Academy of Higher Education, Manipal, Karnataka, India

ARTICLE INFO

Article history:
Received 18 October 2023
Received in revised form 19 November 2023
Accepted 13 December 2023
Available online 30 June 2024

Keywords:
Peristaltic transfer; Casson nano liquid; Heat transfer; Mass transfer

ABSTRACT

This computational study elucidates electromagnetic field effects on peristaltic transport of nanofluids in microfluidic channels using CFD modeling. The feasibility of electroosmotic micropumping for biomedical applications has garnered interest. However, the unique properties and motion of nanofluids warrant investigation. This work examines the impact on peristaltic heat and mass transfer in a non-uniform microchannel geometry incorporating electroosmosis. By explicitly accounting for electroosmotic factors, the coupled PDE system is solved to obtain concentration, temperature and velocity fields. While the electromagnetic simulations prove essential, a key focus lies on electroosmosis phenomena. Effects on parameters including skin friction, Nusselt and Sherwood numbers are analyzed for Casson and Newtonian nanofluids. Visual probing of trapping events further reveals the role of electroosmosis. Overall, this computational approach provides insights into the multifaceted interplay between peristalsis, nanofluids and electroosmotic flows under electromagnetic forces in microfluidic configurations. The perspectives gained at intersection of CFD, biomedical and nanotechnology domains can facilitate optimized designs of electroosmosis-driven biomedical microdevices.

1. Introduction

Current scientific interest in nanofluids has increased in recent years due to the vast number of biological fields in which they can be applied. Magnetic cell separation, chemotherapy, medication delivery, cryotherapy, nano cryosurgery, and cooling technologies are only a few examples. Drug delivery and cooling technology are two further examples. Adding tiny particles, typically with sizes less than 100 nanometers (nm), to conventional heat transfer fluids results in nanofluids. When

* *Corresponding author.*
E-mail address: bs.hadimani@manipal.edu (Balachandra Hadimani)

https://doi.org/10.37934/cfdl.16.11.3759

placed in the right conditions, even a small number of nanoparticles that are contained within the base fluids can dramatically alter the base fluids' thermal characteristics.

The crucial role of nanofluids is effectively established through non-Newtonian fluid models that predict flow behavior. Models such as the Power Law and Carreau-Yasuda describe shear-dependent fluid characteristics. The Herschel-Bulkley, Bingham plastic, and Casson models characterize behavior based on yield stress properties. Current work focuses on the Casson model with nanofluids, capturing viscoelastic fluid properties. Additionally, it provides more accurate representation of flow in notable applications including blood flow analysis, food processes like ketchup and chocolate, and industrial systems like drilling fluids, slurry transport, and equipment design. The Casson nanofluid model has particular significance in accurately predicting complex flows across biological, food, and engineering domains.

Choi [1] revolutionized the field by being the first to propose using nanotechnology in heat transfer fluids to significantly enhance their thermal properties beyond those of their basic fluids. When compared to their respective base fluids, these nanofluids are recognized to possess superior thermal characteristics. Nanofluids are fluids with concentrations below 10 nm, and their purpose is to have good thermal properties at those concentrations. Since Choi's seminal finding, thermal scientists have studied nanofluids, particularly their thermal properties, to determine the underlying processes responsible for their enhanced characteristics. Adopted some interesting investigations from previous studies to explore the current work [6–10]. Further exploring nanofluids, Buongiorno [2] discussed the key roles of thermophoresis and Brownian motion. Alawi *et al.,* [3] examined a nanofluid model for heat transfer enhancement in backward and forward-facing steps. Nadeem and Sadaf [4] reported the influence of single-wall carbon nanotubes with variable viscosity. Additionally, Aman *et al.,* [5] effectively examined the Casson nanofluid model under magnetic field and porosity effects. Current nanofluid research represents a significant advance in technological sophistication, building on previous investigations [6-10]. This work adopts some interesting approaches from earlier studies to explore Casson nanofluid dynamics.

The peristalsis fluid transport process offers various potential applications for nanofluids, which play an important role in many fields. The paper industry, paper production, pharmaceutical, chemical, and cosmetic sectors all rely heavily on the process of peristalsis, which is initiated when a wave travels down the walls of a tube or duct. In biological systems, this peristaltic mechanism may be involved in controlling blood flow, urine flow, and digestion of food, oocyte transfer, and sperm movement. Many different types of medical devices use peristaltic pumps, such as dialysis machines, infusion pumps, and open-heart bypass pumps. Latham [11] was ahead of his time when studying fluid dynamics. His seminal research focused on how peristaltic action propels urine through the ureter. Since then, many scientists have tried to decipher the intricacies of peristalsis in non-Newtonian and Newtonian fluids by employing many hypotheses [12–15]. Akbar and Nadeem [16] deserve special recognition for being the first to include nanofluids in peristaltic pumping models. Mustafa *et al.,* [17] used analytical and computational techniques to investigate how wall characteristics affect peristaltic nanofluid flow. The Homotopy Perturbation Method (HPM) was used as one example of a computational technique. Similarly, Akbar*et al.,* [18] studied the peristaltic flow of nanofluids and their effect on heat transfer within an asymmetric channel. Moreover, Kothandapani and Prakash [19] looked at how magnetic fields and heat radiation affected nanofluids as they flowed through a tapered symmetric duct embedded in a porous medium. Natural convection within a deformable, porous vertical layer containing Jeffrey liquids was studied by Sreenadh*et al.,* [20]. The impact of magnetic fields on peristaltic transport is significant in biomedicine because of the prevalence of magnetic resonance imaging (MRI), the use of magnetic particles in medicine transport, and the reliance of medical machinery on magnetic fields for drug delivery and cancer

therapy [21]. Utilizing the magnetic characteristics of nanoparticles and nanoliquids based on iron allows for delivering non-lethal radiation to cancer patients receiving treatment. Incorporating Brownian motion and thermophoresis into our understanding of nanofluids has also led to significant advancements in the field of research. Based on that, we refereed previous examinations from [22–29].

Extensive research into electroosmosis has revealed its considerable importance in various fields, including fluid mechanics and microfluidics. Advances in chromatography, electrophoresis, and the precise control of fluids in microscale systems can all be attributed to this phenomenon. Electroosmosis can be defined as the movement of a liquid through a porous medium with the aid of an external electric field. When an electric field comes into contact with charged particles in a fluid, a phenomenon known as electric field-induced current is produced. The phenomenon is the result of this interaction. A great many real-world accomplishments can be traced back to this phenomenon. When an electric field comes into contact with a surface, the surface becomes electrically conductive. The particles predictably displace the liquid because of the adhesive drag that suddenly causes the liquid to rise to the surface. When the electrolyte comes into touch with the character, particles begin to accumulate in a continuous web. Several studies in the field have examined the impact of electroosmosis on fluid dynamics.The effect of mixed convection on nano-bio-fluid and its interaction with an applied electric field during wave propagation in curved channels was studied, for instance, by Ijaz *et al.,* [30]. The researchers here aimed to learn more about wave movement. Similar research was conducted by Tripathi *et al.,* [31], who studied the intricate peristaltic wave propagation created in microchannels by buoyancy effects in electroosmosis. In addition, Hussain *et al.,* [32] found that the peristaltic flow of PTT (Phan-Thien-Tanner) fluid was affected by electroosmotic force. These are merely a sampling of the many observations made in the field. Few more interesting investigations are considered to enhance the role of current work [33–39].

Our current research is motivated by previous discussions, and it aims to learn more about the electromagnetic peristaltic transport of non-Newtonian Casson nanofluids inside a non-uniform conduit with slip boundary conditions. The Casson fluid model successfully represents blood circulation within the arteries and veins. One of the non-Newtonian models that help us comprehend the complex rheological behavior of biological fluids is the Casson fluid model. Our research uses dimensionless parameters to characterize the flow while assuming long wavelengths and low Reynolds numbers. The solution of these governing equations sheds light on the phenomenon. Finally, we provide a graphical comparison of our results across all the physical parameters we considered. This article's research has real-world applications in medicine, biomedical engineering, and technology. In the medical field, where understanding such flow dynamics is crucial, the insights it provides into the behavior of biological fluids under the effect of peristalsis are invaluable.

2. Formulation of the Problem

Consider two-dimensional peristaltic flow of non-Newtonian Casson nanofluid in a non-uniform vertical channel (see Figure 1). A constant temperature maintained at the flexible walls of the channel. λ be the wavelength of the sinusoidal wavewhich trains variations with accelerating velocity as it travels down the channel. The geometry of the non-uniform channel is expressed below:

$$h = 1 + mx + \varepsilon \cos\left(\frac{2\pi}{\lambda}(x - ct)\right) \tag{1}$$

Where, m, t, c, εrepresents the non-uniform parameter,time, wave speed and amplitude of the peristaltic wave respectively.In a frame of reference in motion, assuming that the fluid flow remains constant across time is justifiable, yet the flow cannot be regarded as stable in a stationary frame. The correlated transformations between stationary coordinates $(\overline{X}, \overline{Y})$ and moving coordinates $(\overline{x}, \overline{y})$ are

$$\overline{x} = \overline{X} - c\overline{t},\ \overline{y} = \overline{Y},\ \overline{p} = \overline{P}(x,t), \overline{u} = \overline{U} - c,\ \overline{\chi} = \overline{\psi} - \frac{R^2}{2} \tag{2}$$

Where$\overline{P}$**,** $\overline{\chi}$and$\overline{U}$aredimensional pressure, stream function and velocity are identified as stationary coordinates. Similarly, $\overline{p}$, $\overline{\psi}$and$\overline{u}$are in the dimensionless pressure, stream function and velocity which are identified as moving coordinates.

For an incompressible flow of the Casson nanofluid, the following expression represents the rheological equation of stress:

$$\tau_{ij} = \begin{cases} 2\left(\mu_B + \frac{P_y}{\sqrt{2\pi}}\right) e_{ij} & \pi > \pi_c \\ 2\left(\mu_B + \frac{P_y}{\sqrt{2\pi_c}}\right) e_{ij} & \pi < \pi_c \end{cases} \tag{3}$$

Where, $\mu_B$represents the plastic dynamic viscosity, π denotes the product of the component of deformation rate with itself i. e. $\pi = e_{ij}e_{ij}, e_{ij} = \frac{1}{2}\left(\frac{\partial u_i}{\partial x_j} + \frac{\partial u_j}{\partial x_i}\right)$is rate of strain component, the Casson yield stress expressed as$P_y = \frac{\mu_B\sqrt{2\pi}}{\beta}$, where β denotes the Casson fluid parameter and$\pi_c$is the critical value of π based on a non-Newtonian model.

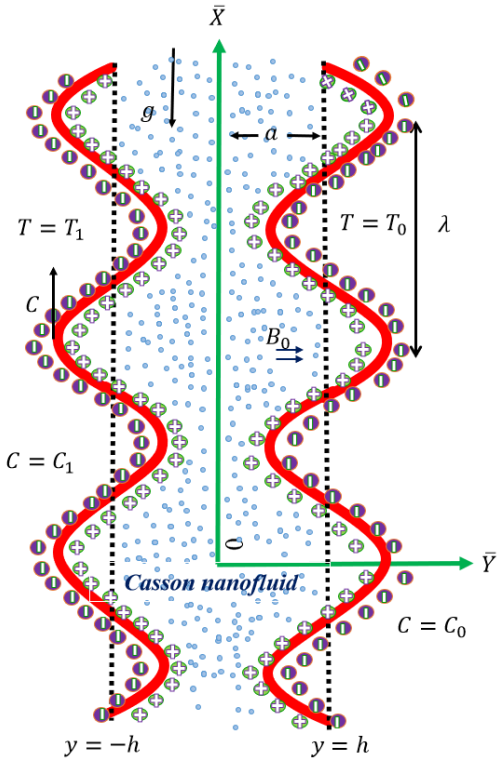

Fig. 1. Geometry of the fluid flow

The equations for 2-D flow model [5] are:

$$\mu\left(1+\frac{1}{\beta}\right)\frac{d^2\overline{u}}{d\overline{y^2}}-\sigma B_0^2(\overline{u}+c)+(1-C_0)\rho_{f_0}g\beta^*(T-T_0)+(\rho_f-\rho_{f_0})g\beta^*(C-C_0)+\rho_e\overline{E}_{\overline{x}}=\frac{d\overline{p}}{d\overline{x}} \quad (4)$$

$$k\frac{d^2T}{d\overline{y^2}}+(\rho c)_p\left[D_B\frac{dC}{d\overline{y}}\frac{dT}{d\overline{y}}+\frac{D_T}{T_0}\left(\frac{dT}{d\overline{y}}\right)^2\right]+\mu\left(\frac{d\overline{u}}{d\overline{y}}\right)^2+\sigma B_0^2(\bar{u}+c)^2=0 \quad (5)$$

$$D_B\frac{d^2C}{d\overline{y^2}}+\left(\frac{D_T}{T_0}\right)\frac{d^2T}{d\overline{y^2}}=0 \quad (6)$$

Where $\beta=\sqrt{\frac{2\pi_c}{P_y}}$is the Casson fluid parameter,

With respect to the flow geometry, the following boundary conditions are assumed

$$\frac{d\overline{u}}{d\overline{y}}=0,\ \frac{dT}{d\overline{y}}=0,\ \frac{dC}{d\overline{y}}=0 \text{ at } y=0, \quad (7)$$

$$\overline{u}+\alpha_1\frac{d\overline{u}}{d\overline{y}}=-c, T+\alpha_2\frac{dT}{d\overline{y}}=T_1, C+\alpha_3\frac{dC}{d\overline{y}}=C_1 \text{at} y=h. \quad (8)$$

Where, $(\overline{x},\overline{y})$are dimensional coordinates. $p,\theta,Br,Mn,Re,Pr,\Theta,Ec,C_p$ denotes the pressure, temperature, Brickman number, Reynolds number, Prandtl number, volume flow rate and Eckert number, applied magnetic field and the specific heat at a constant pressure respectively.

The relevant dimensionless quantities can be described as

$$x=\frac{\bar{x}}{\lambda},y=\frac{\overline{y}}{a},u=\frac{\overline{u}}{c},t=\frac{c\overline{t}}{\lambda},p=\frac{\bar{p}a^2}{\lambda\mu c},\varepsilon=\frac{b}{a},Re=\frac{\rho ca}{\mu},Pr=\frac{\mu c_p}{k},\lambda_D=\frac{1}{ez_v}\sqrt{\frac{T_0\varepsilon K_H}{2n_0}},\delta=\frac{c}{\lambda'},$$

$$\theta=\frac{T-T_0}{T_1-T_0},\phi=\frac{C-C_0}{C_1-C_0},h=\frac{H}{a},Mn=\sqrt{\frac{\sigma}{\mu}}B_0a,Nb=D_B\frac{(\rho c)_p(C_1-C_0)}{k},Br=Ec\,Pr,$$

$$Gr=\frac{(1-C_0)g\beta^*(T_1-T_0)a^2}{\vartheta^2},G=\frac{Gr}{Re},Nt=D_T\frac{(\rho c)_p(T_1-T_0)}{T_0k},B=\frac{(\rho_f-\rho_{f_0})(C_1-C_0)g\beta^*a^2}{\mu c},$$

$$Ec=\frac{c^2}{c_p(T_1-T_0)},\phi=\frac{ez_v}{T_{av}K_B}\overline{\phi},U_{hs}=-\frac{E_1\varepsilon}{c\mu}.$$

Where, $(x,y),\mu,m_e,\ \lambda_D,\ U_{hs},Gr,Nt,Nb,D_T,D_B,z_v,K_B,e,T_{av}$represents the dimensionless co-ordinates,dynamic viscosity, electroosmosis parameter, Debye length, Helmholtz-Smoluchowski velocity, Grashof number, Thermophoresis parameter, Brownian motion parameter, Thermal diffusion coefficient, Brownian motion diffusion coefficient, charge balance, Boltzmann constant, electronic charge and the average temperature respectively.

The fundamental governing Eq. (4) – Eq. (6), as well as the boundary conditions Eq. (7) and Eq. (8), may be simplified using the dimensionless parameters indicated beforehand:

$$\left(1+\frac{1}{\beta}\right)\frac{d^2u}{dy^2}+G\theta-Br\Phi-Mn^2(u+1)+me^2U_{hs}\phi=\frac{dp}{dx} \quad (9)$$

$$\frac{d^2\theta}{dy^2}+Nb\frac{d\theta}{dy}\frac{d\Phi}{dy}+Nt\left(\frac{d\theta}{dy}\right)^2+Br\left(\frac{du}{dy}\right)^2+BrMn^2(u+1)^2=0 \quad (10)$$

$$\frac{d^2\Phi}{dy^2}+\frac{Nt}{Nb}\frac{d^2\theta}{dy^2} \quad (11)$$

Accordingly, the established boundary conditions are

$$\frac{du}{dy}=0,\frac{d\theta}{dy}=0,\frac{d\Phi}{dy}=0 \quad \text{at} y=0, \quad (12)$$

$$u+\alpha_1\frac{du}{dy}=-1,\theta+\alpha_2\frac{d\theta}{dy}=1,\Phi+\alpha_3\frac{d\Phi}{dy}=1 \ \text{at} y=h. \quad (13)$$

In the above equation, $\alpha_1,\alpha_2,\alpha_3$, Mnrepresents the velocity slip parameter, thermal slip parameter and concentration slip parameter, magnetic field parameter respectively.

3. Solution

3.1 Potential Distribution

The Poisson equation $\left(\nabla^2\bar{\phi}=-\frac{\rho_e}{\varepsilon}\right)$is used to describe the electric potential in the microchannel. The net charge density $\rho_e$follows the Boltzmann distribution, which is given by the following relation:

$$\rho_e=-z_ve(\bar{n}^-+\bar{n}^+). \quad (14)$$

Here, the anions $(\bar{n}^-)$and cations $(\bar{n}^+)$are defined through $\rho_e$of the Boltzmann equation are as follows:

$$\bar{n}^{\pm}=n_0e^{\left(\pm\frac{ez_v}{T_{av}}\bar{\phi}\right)} \quad (15)$$

Where $n_0$is the bulk concentration, $z_v$is the charge balance, $K_B$is the Boltzmann constant, e is the electronic charge, and $T_{av}$is the average temperature. Applying Debye-Huckellinearization approximation, we get:

$$\frac{d^2\Phi}{dy^2}=m_e^2\Phi \quad (16)$$

Here, $m_e$is the electroosmotic parameter. The analytical solution of the above Eq. (16) as follows:

$$\Phi(y)=\frac{Cosh(m_ey)}{Cosh(m_eh)} \quad (17)$$

Solving Eq. (9) – Eq. (11) analytically might be difficult as they are non-linear coupled equations. Thus, the newly formed governing equations are addressed analytically by utilizing corresponding boundary conditions Eq. (12) – Eq. (13) through MATHEMATICA software via. ND Solve technique.

The relationships for wall shear stress, the Nusselt number, and the Sherwood number, which, respectively, characterize the rates of heat and mass transport, are as follows:

$$C_f = h' \frac{d^2\psi}{dy^2}\Big|_{y=h} \tag{18}$$

$$Nu = h' \frac{d\theta}{dy}\Big|_{y=h} \tag{19}$$

$$Sh = h' \frac{d\Phi}{dy}\Big|_{y=h} \tag{20}$$

Based on the relationships mentioned above, $h' = m + \frac{2\pi\varepsilon}{\lambda} sin[2\pi(x-t)]$, stream function $(\psi)$is defined as

$u = \frac{d\psi}{dy}$. (21)

The relationship among mean flow $(\Theta)$is connected with certain fixed ordinates, which is tied to movable references $F$and is represented by $\Theta = F + 1$ where;

$$F = \int_0^h u dy \tag{22}$$

Solving equations (9), we get for $\frac{dp}{dx}$. (23)

The non-dimensional pressure rise obtained by using Eq. (23) and the relation mentioned below:

$$\Delta p = \int_0^1 \frac{dp}{dx} dx \tag{24}$$

4. Graphical Results and Discussions

This section's goal is to use graphs to illustrate how pertinent terms behave on a range of physiological values for both Newtonian and non-Newtonian Casson fluids. In the case of Newtonian fluids$\left(\frac{1}{\beta} \to 0\right)$ and Casson nanofluids$(\beta = 1)$, the value $\beta$is always the same. The goal of this work is to shed light on the important distinctions between Newtonian and non-Newtonian fluids. Furthermore, the figures demonstrate that the Newtonian liquid's temperature and velocity are higher than those of the Casson fluid; nonetheless, the concentration shows a pattern that defies expectation. The results have significant ramifications for the commercial sector as well as the field of medicine.

Figure 2 displays the validation results for velocity, temperature, concentration, and pressure rise versus mean flow of the liquid flow for this study conducted by Srinivas *et al.,* [5], by setting Electromagnetic term tends to zero $(E_x \to 0)$, $\frac{1}{\beta} = 0$, $\alpha_1 = 0$, $\alpha_2 = 0$ and $\alpha_3 = 0$. This was done to compare the results to the fluid's mean flow rate after the investigation was complete.

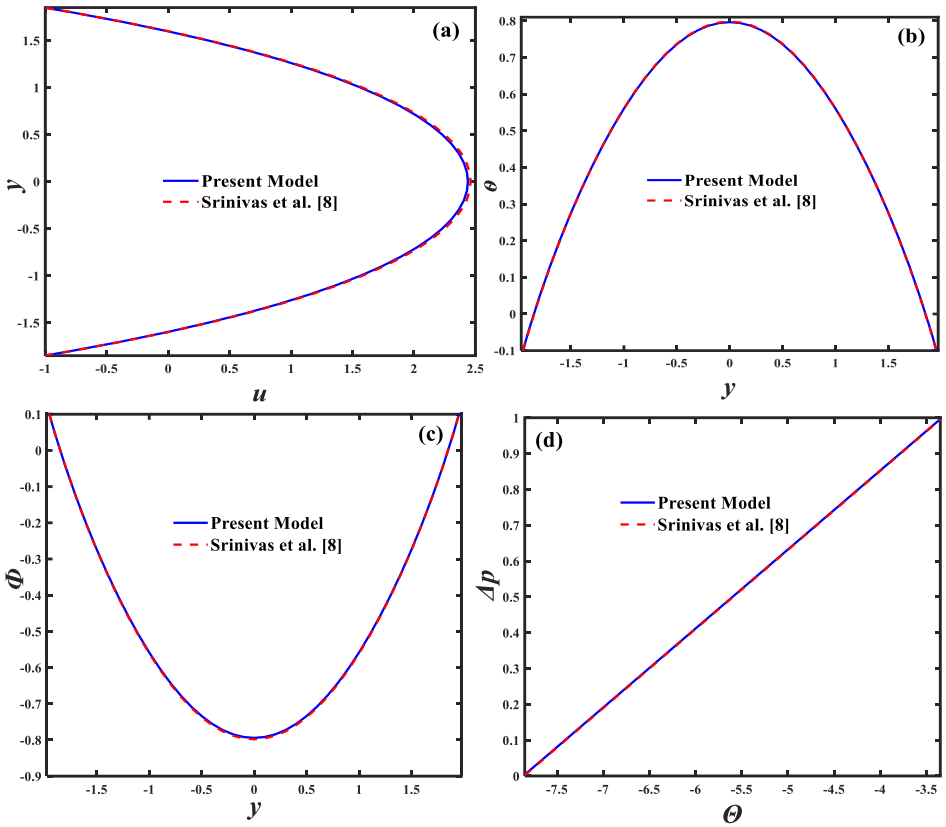

Fig. 2. Graphs demonstrating the validity of the velocities, temperatures, concentrations, and pressure rises on the mean flow profile

4.1 Velocity Profiles

This subsection aims to investigate the influence of different parameters on the velocity profile, as shown in Figures 3(a) through (j). The velocity distributions have the signature parabolic shape, with the maximum velocity at the curve's apex. The influence of the magnetic field on speed is explored in Figure 3(a). As the magnetic parameter drops, the velocity increases due to the Lorentz force acting in opposition to the magnetic field. The effect of the non-uniformity parameter on the velocity of the flow is studied in Figure 3(b). It's clear that the velocity drops in a restricted channel and rises in a wider channel facing the opposite direction. Liquid velocity is shown to be affected by the thermophoresis parameter, as seen in Figure 3(c). Increases in the thermophoresis term value result in greater liquid velocities. Because, higher the thermophoresis can lead to greater heat radiation in system along with increases the fluid flow. In addition, a radiated heat shrinks the Brownian motion effect on velocity profile which is depicted in Figure 3(d). The velocity of the fluid drops as the Brownian motion term rises. The electroosmotic force is a result of the Coulomb force, which is created when an electric field charges a solution. Hence, the velocity profile in Figure 3(e) rises as the electric field strength increases. Figure 3(f) depicts the impact of the Grashof number on the velocity profile. As the Grashof number increases, buoyancy and radiation effects slow the fluid down, causing the fluid to move more slowly. The influence of the Brickman number on the speed of a nanoparticle is investigated in Figure 3(g). Here, it can be seen that raising the Brickman number slows down the flow of the fluid. The Reynolds number has an effect on the liquid's velocity, as seen in Figure 3(h). The velocity of a fluid increases as the Reynolds number decreases Figure 3(i) demonstrates that the contour flattens out when the velocity slip rises. Because, the velocity slip can alter the drag force impact on fluid due to variation in shear stress distribution in the media. Finally,

the effect of the Helmholtz-Smoluchowski parameter on the velocity profile indicates that the curve flattens out with increasing Helmholtz-Smoluchowski value which is depicted in Figure 3(j).

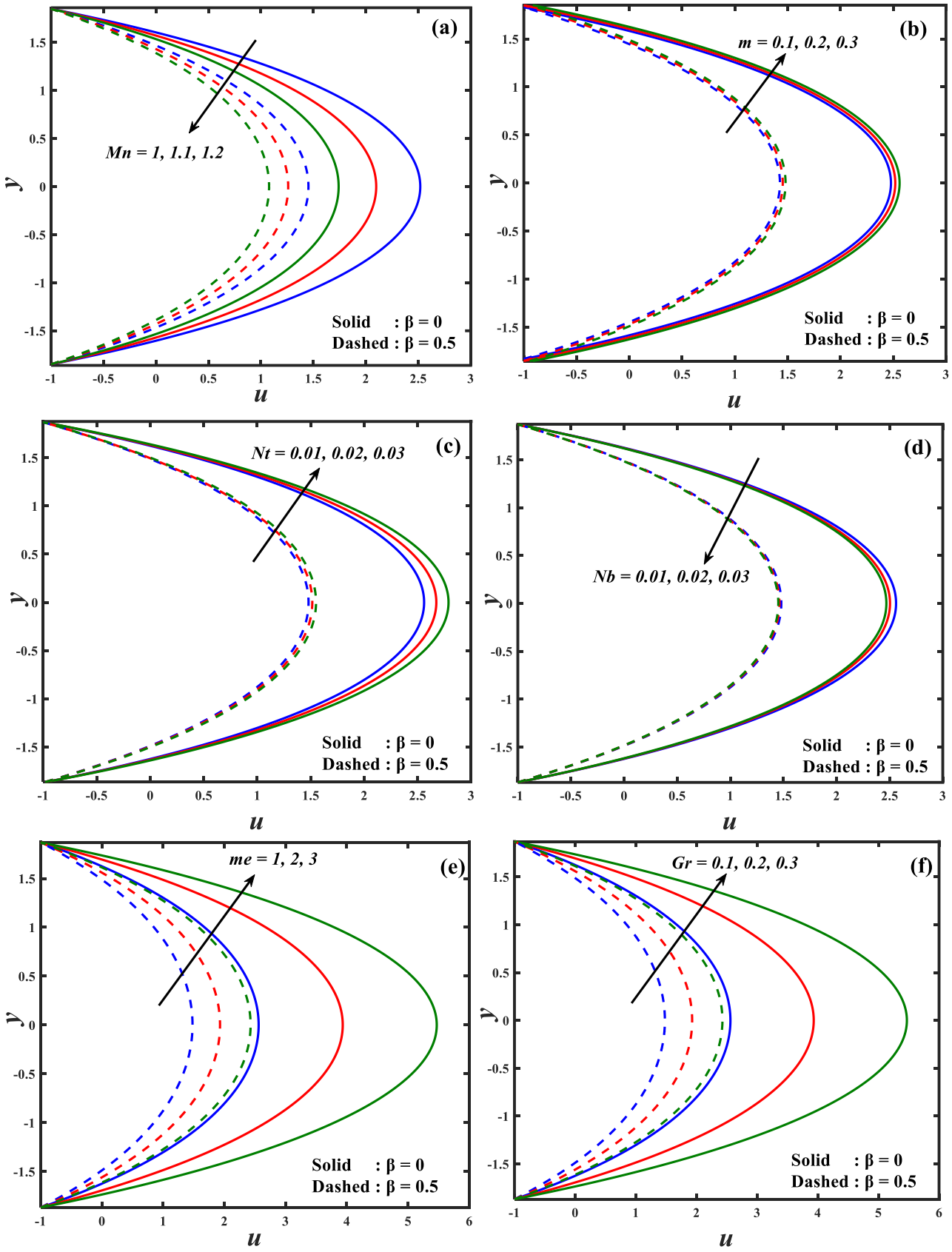

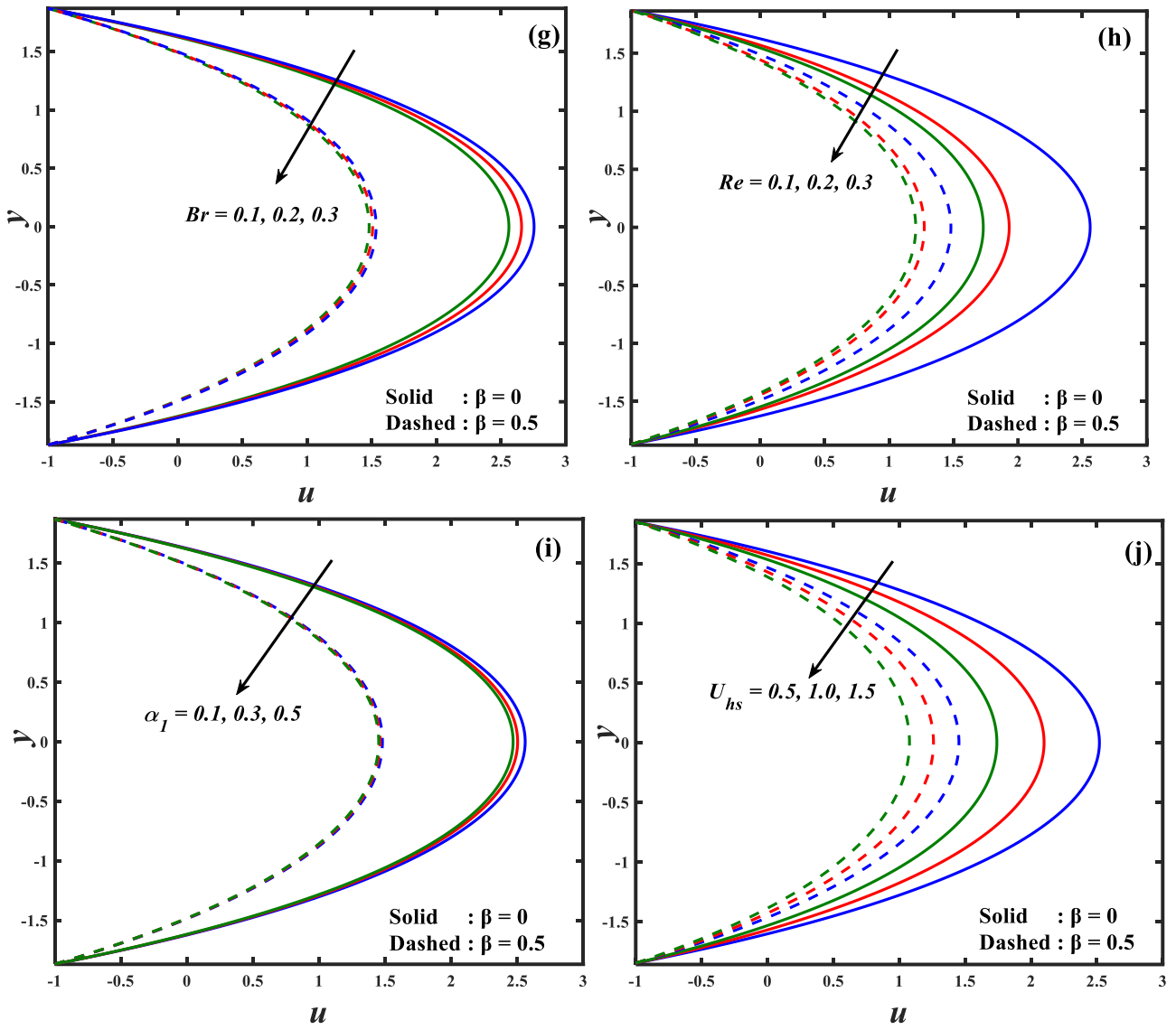

Fig. 3. Velocity profiles for various values of (a) *Mn*, (b)*m,* (c)*Nt,* (d)*Nb,*(e) *me*, (f) *Gr,* (g)*Br,* (h)*Re,* (i) $\propto_1$, (j) U_{hs}

4.2 Temperature

Using Figures 4(a)-(h), we analyze the relationship between temperature and other important fluid characteristics. Like velocity profiles, temperature profiles have a recognizable parabolic shape, with the peak temperature located in the profile's center. As shown in Figure 4(a), the fluid temperature drops as the value of the magnetic field parameter increases. Because, the flow of the fluid reduces due to the thermal expansion. Figure 4(b) shows, on the other hand, that as the thermal slip parameter is increased, the temperature profile also rises. The effect of the non-uniformity parameter on temperature distributions is illustrated in Figure 4(c). According to this theory, the fluid's temperature drops as the channel gets narrower and rises as it gets more curved. Figure 4(d) displays the temperature distribution as a function of the Helmholtz-Smoluchowski number. As the Helmholtz-Smoluchowski number grows, so does the temperature of the fluid. The Grashof number clearly shows a linear correlation with temperature, as seen in Figure 4(e). This is because an increase in the Grashof number also increases the temperature by making the temperature gradient stronger. In addition, maximum Grashof number can increase the velocity of the nanofluids. A Brickman number act as an effective conductor between wall and the fluid, due to the low conduction the heat

transfer reduces effectively. Figure 4(f) illustrates how the Brickman number of a nanoparticle affects the space around it. As the Brickman number rises, the temperature naturally falls. The reason behand this situation is that when we enhancing the Brickman number, it reduces the conduction of heat created by viscous dissipation and hence the temperature decreases significantly. Figure 4(g) delves into the relationship between the Reynolds number and the liquid's temperature. Here, the liquid's temperature rises with decreasing Reynolds number. Finally, as the electric field strength increases, the temperature profile drops, as shown in Figure 4(h).Due to variation of Debye length can leads to reduction in electroosmotic force.

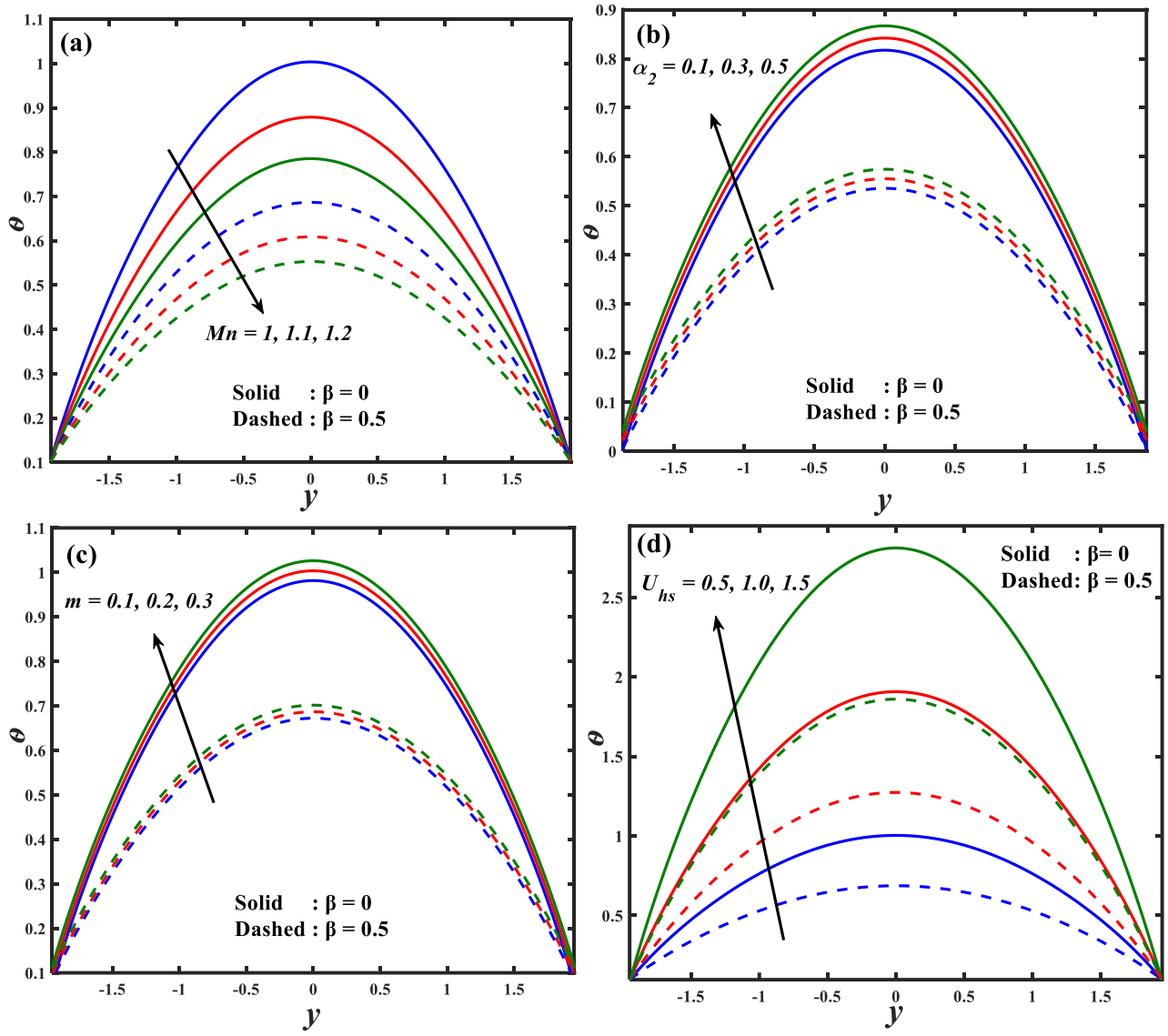

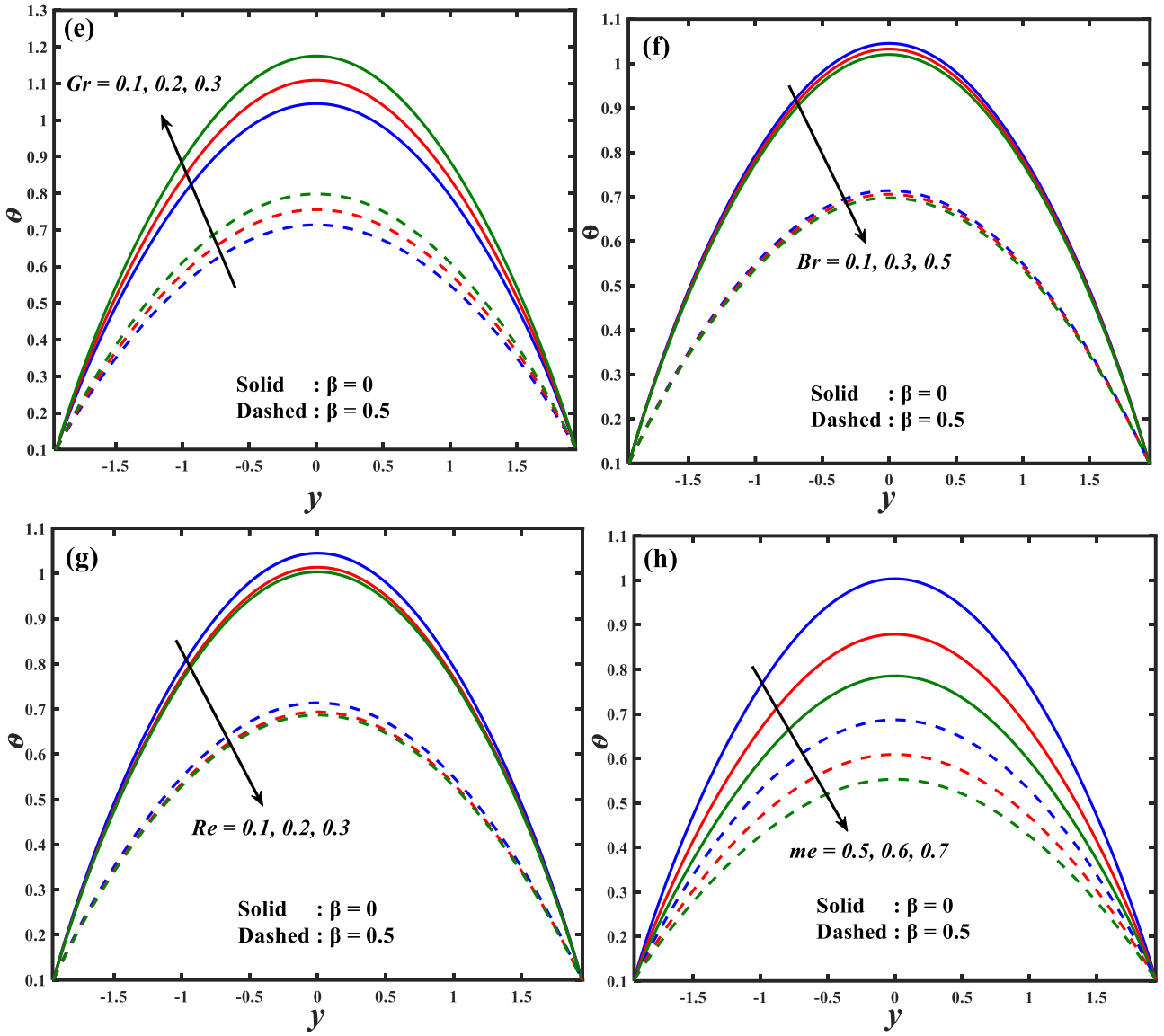

Fig. 4. Temperature profiles for various values of (a) *Mn*(b) $\propto_2$, (c)*m*(d)U_{hs}(e) *Gr* (f)*Br* (g)*Re,* (h) *me*

4.3 Concentration Profiles

Here, we explore the shown in Figures 5(a) to (h) fluctuations in nanoparticle concentration within the Casson fluid as a function of these important parameters. Like the velocity and temperature profiles, the concentration profile is parabolic. Figure 5(a) shows that the concentration of nanoparticles in the fluid drops as the magnetic field value decreases. Figure 5(b) shows, on the other hand, that concentration grows as the concentration slip parameter increases. The effect of varying the non-uniformity parameter on the concentration profile is seen in Figure 5(c). The concentration is observed to be the lowest in a broader channel, flowing in the opposite direction and highest inside a narrow channel. Figure 5(d) displays the effect of varying the thermophoresis parameter on the concentration. Here, it can be noted that a larger thermophoresis term results in less liquid being present in the vertical channel. Due to the non-uniform surface associated with nanoparticles, the concentration of boots up while considering the Brownian motion effect, which enhances the velocity but falls the thermophoresis impact on concentration profile. Concentration changes as a function of Brownian motion parameter adjustments are depicted in Figure 5(e). It can be shown that as the Brownian movement term grows, so does the liquid's concentration. Fluid

concentration is seen to increase with the Grashof number as well. The influence of the Reynolds number on the fluid concentration in a region is depicted in Figure 5(f). As the Reynolds number goes down, the concentration of the liquid goes up, as shown in the image. Concentration is shown to be affected by the Grashof number, as seen in Figure 5(g). It has been found that the volume of fluid contained within a vertical channel decrease as the Grashof number rises.In addition, Grashof number associated with buoyancy force and thermal impact which results in such declining distribution on concentration profile.Finally, concentration changes for several values of the local Brickman number are depicted in Figure 5(h). Concentration levels are shown to correlate with an increase in the Brickman number.

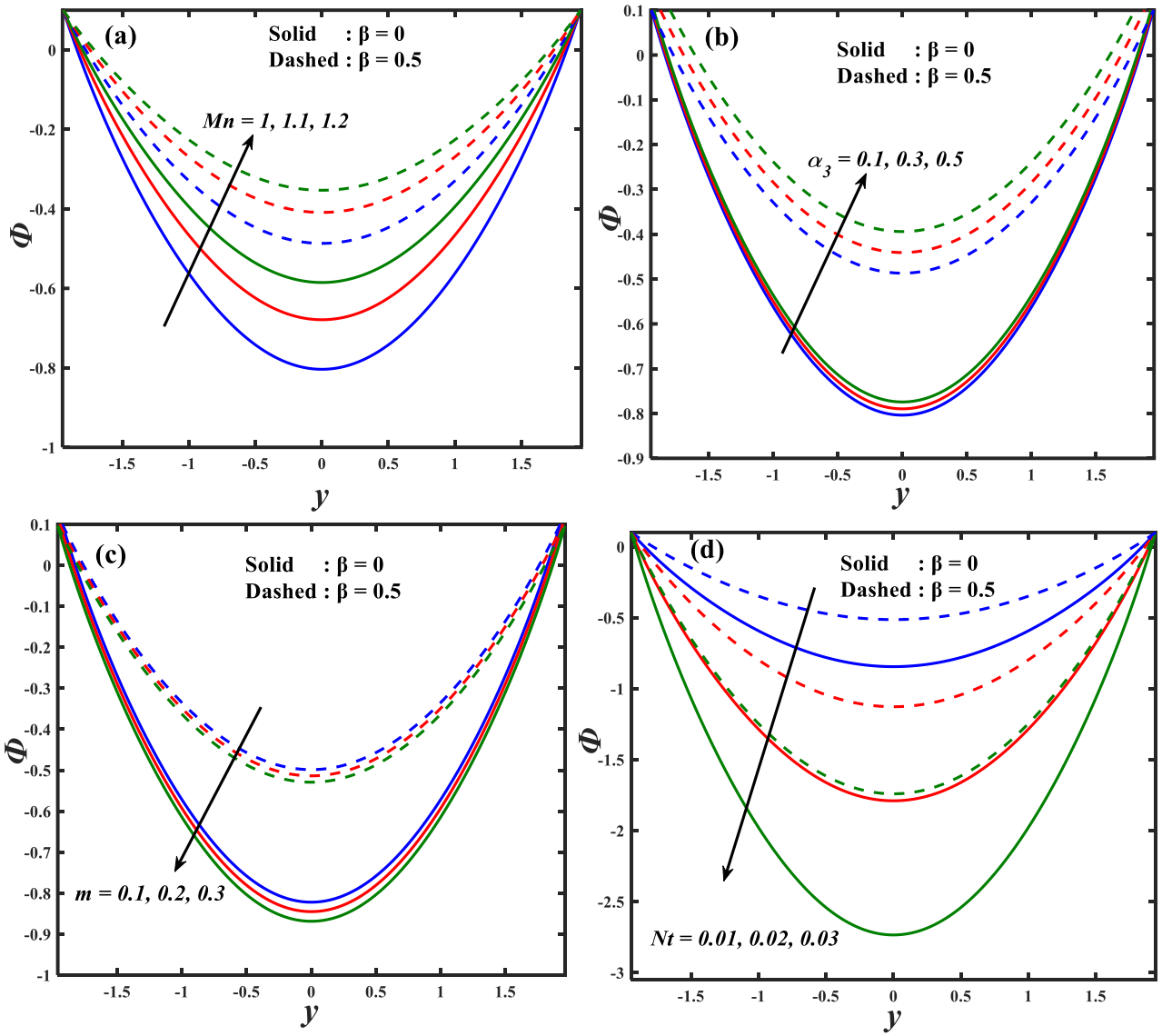

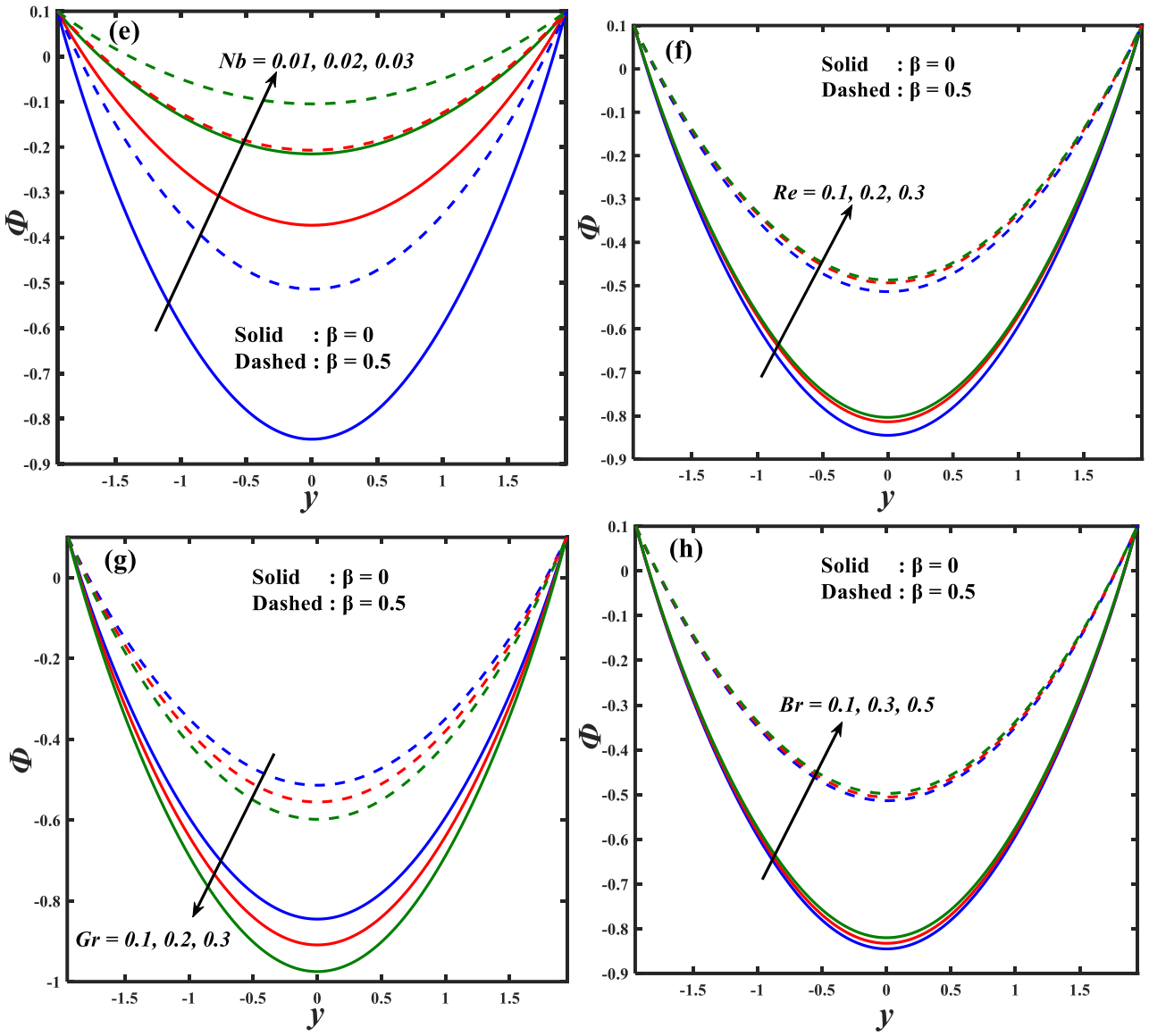

Fig. 5. Concentration profiles for various values of (a) *Mn,* (b) $\propto_3$, (c) *m*, (d) *Nt*, (e) *Nb,*(f) *Re*(g) *Gr,* (h) *Br*

4.4 Effect of Physical Quantities

Shear stress, heat transport rate (expressed by the Nusselt number), and mass transport rate (represented by the Sherwood number) along the channel walls are all affected by the flow of a real fluid through a channel. The study of these physiological markers is crucial because of the many areas in which they might be helpful. In the case of atherosclerotic plaques, for instance, oscillatory shear stress may play a role in minimizing their severity. Furthermore, the Nusselt and Sherwood numbers exhibit oscillatory behavior because the walls of the channel contract and expand due to the peristaltic motion of the liquid within the channel. The fluid's characteristics may be affected by this swaying. Figures 6, 7, and 8 show the range of values for various physical constants over which we investigate the skin friction coefficient, Nusselt number, and Sherwood number, respectively. Figures 6 and 7 indicate that the skin-friction coefficient and the Nusselt number rise as the magnetic field parameter decreases. Figure 8 shows that the Sherwood number goes in the opposite direction as the magnetic field parameter falls. The results of changing the electric field and the Helmholtz-Smoluchowski parameters are shown in Figure 6 and Figure 7. As shown in Figure 6, when the Helmholtz-Smoluchowski parameter rises, the skin-friction coefficient falls, whereas Figure 7 shows

the Nusselt number increases. Figure 6 also shows how the skin friction coefficient changes with different thermophoresis and Brownian movement parameter values. The skin friction coefficient increases with an increase in the thermophoresis parameter and decreases with an increase in the Brownian movement term. Figure 8 shows that the Sherwood number exhibits the inverse behavior for these parameters. Figures 7 and 8 finally demonstrate the impact of the Brickman number (Br). Figure 7 shows that as the Brickman number increases, the Nusselt number also rises, while Figure 8 demonstrates that the Sherwood number falls under the same circumstances.

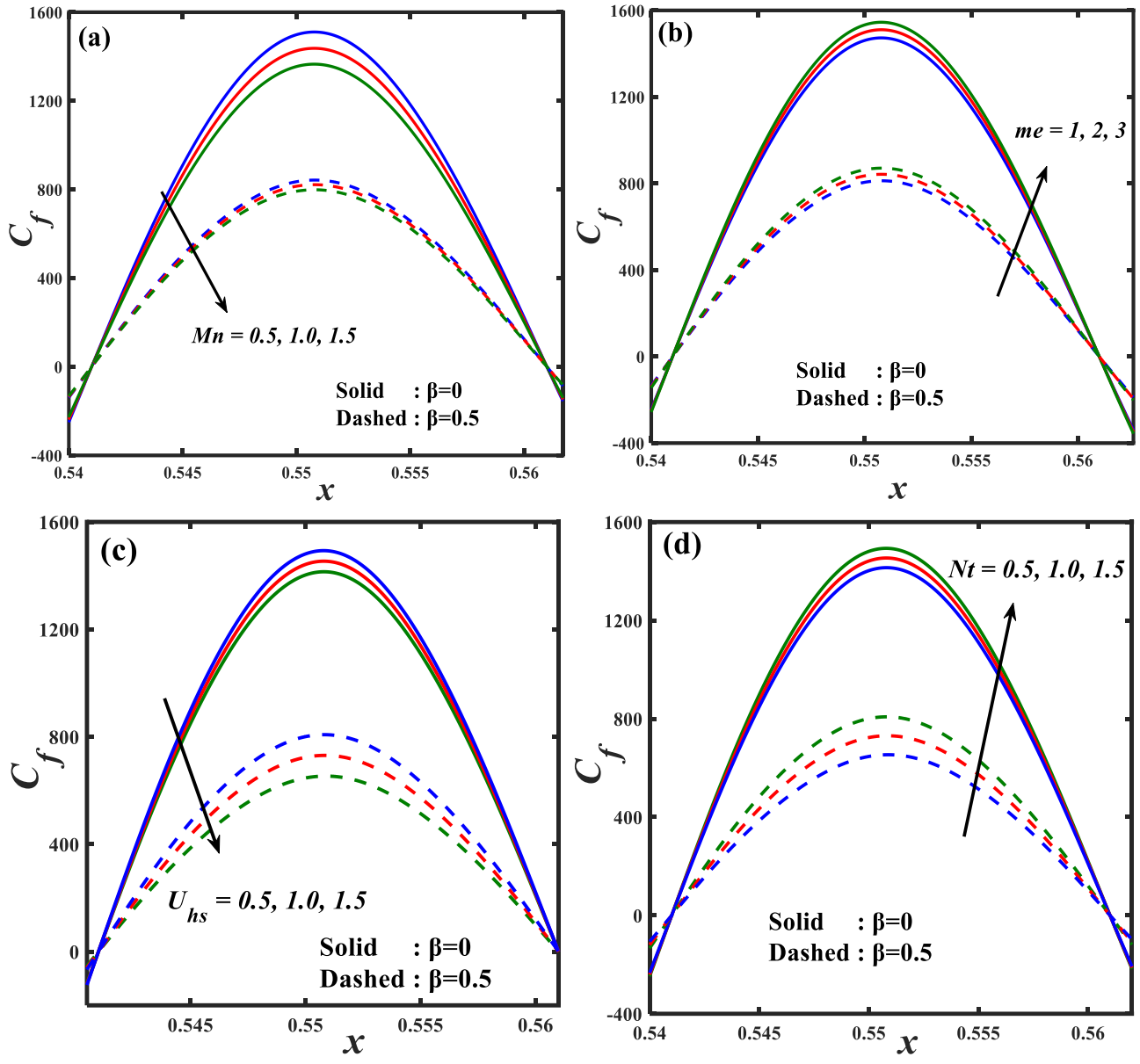

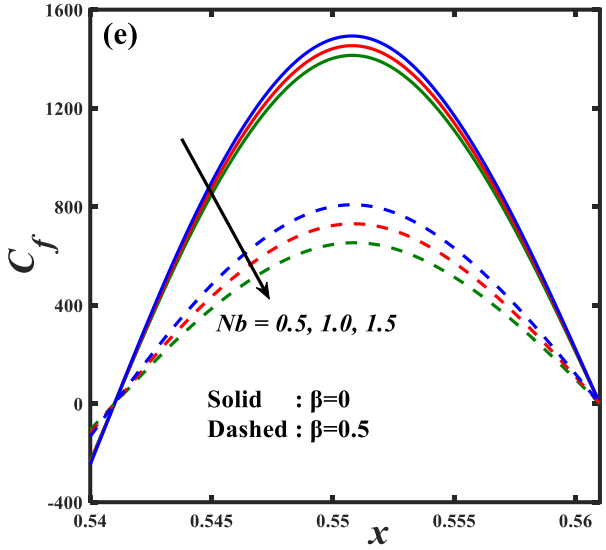

Fig. 6. Variation in C_f, for various physical constraints(a) *Mn, (b) me, (c) U_{hs}, (d) Nt, (e) Nb*

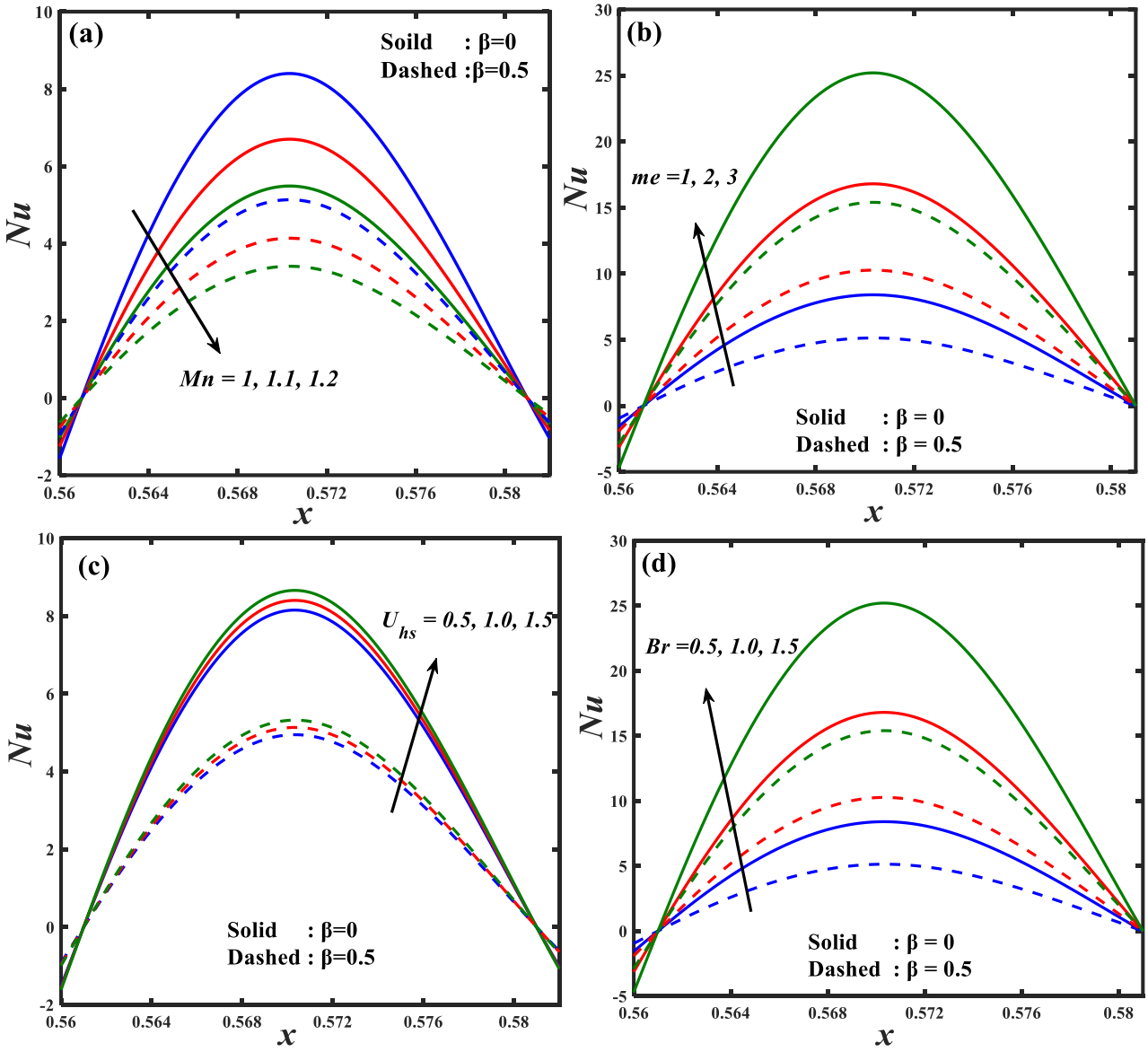

Fig. 7. Variation in *Nu* for various physical constraints (a) *Mn, (b) me, (c) U_{hs}, (d) Br*

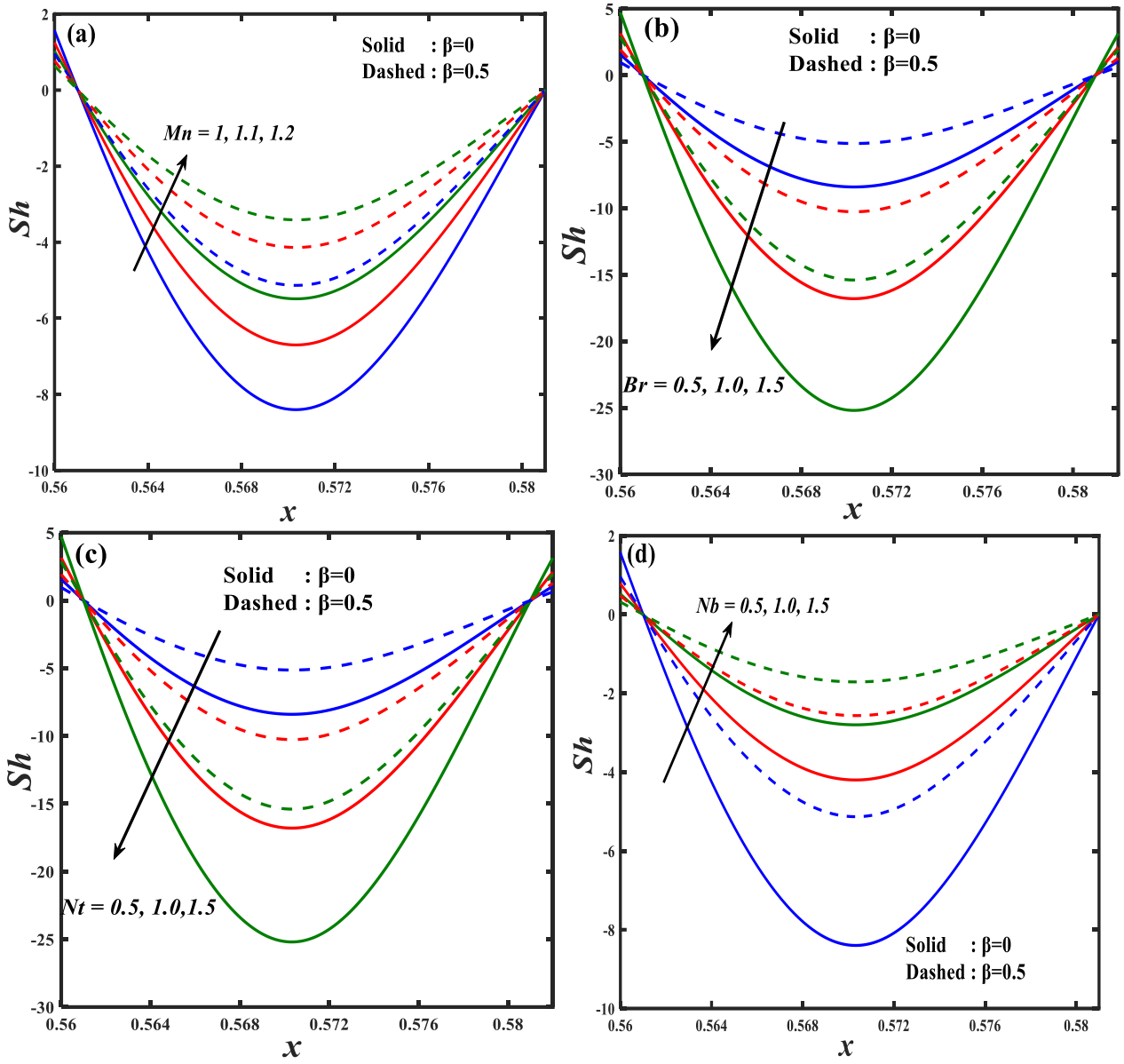

Fig. 8. Variation in*Sh* for various physical constraints (a) *Mn, (b) Br, (c) Nt, (d) Nb*

4.5 Pressure-rise versus Mean Flow

Understanding how a pump works is crucial to learning about the physics of biofluids in the context of peristalsis. The fluid displacement during contractions drives the pumping action, which is caused by the significant pressure produced by the walls. Observing the pressure rise or fall of the typical flow rate over time might provide light on the workings of a pump. It has long been known that the linear and inverse proportional relationship between the pressure rise and the mean flow rate over time holds. Furthermore, the range of values greatly affects the behavior of numerous physical characteristics. Figures 9(a) through (e) show the relationship between the mean flow rate and the pressure rise for a range of values of the physical parameters in question. Figure 9(a) shows that when the average flow rate increases, the pressure rise reduces; this effect is more prominent in Casson fluid than Newtonian fluid. On the other hand, as seen in Figure 9(b), pressure increases as magnetic field parameter values increase. Figure 9(b) demonstrates, on the other hand, that as electric field parameter values are reduced, the resulting pressure rise is also reduced. Figure 9(c)

shows that as the Helmholtz-Smoluchowski term is increased, the pressure increases; this impact is expected to decrease for Newtonian fluid and increase for non-Newtonian fluid. Pressure decreases as the thermophoresis parameter increases, as seen in Figure 9(d), illustrating the impact of the thermophoresis term. Figure 9(e) depicts the reverse tendency, with the Brownian motion parameter increasing the pressure rise.

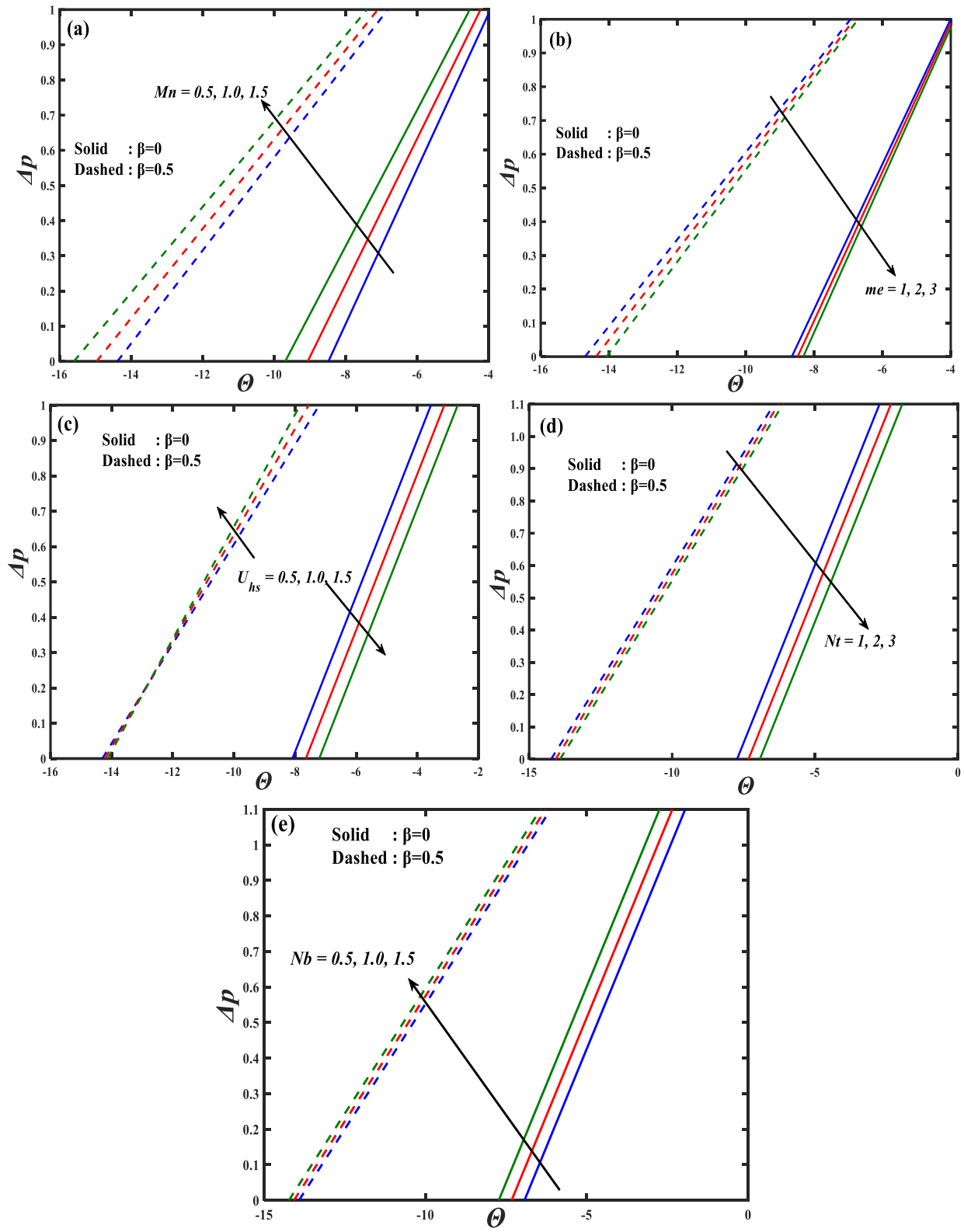

Fig. 9. Pressure riseversus mean flow for (a) *Mn,* (b) *me, (c)* U_{hs} (d) *Nt* (e) *Nb*

4.6 Trapping Phenomena

Trapping is a unique hydrodynamic feature of the peristaltic process, particularly when an application of a large amplitude ratio is made. This impact reorganizes the bolus in the fluid flow in an irregular fashion. Stream functions are used to quantify the trapping phenomena by measuring the movement of a bolus through a "trapping" fluid. In reaction to the peristaltic wave, boluses move in a sinusoidal pattern, yet in rare situations, the spherical bolus takes on a fixed-frame structure due to the splitting of specific streamlines. The peristaltic wave completely encircles the bolus, carrying it along at speed. Figure 10 shows how the magnetic field term affects the trapped bolus. As the magnetic field parameter increases, it is seen that the size and number of trapped boluses decrease for weak streamline circulations. The force of a magnetic field can be used to control the growth of boluses. Changes in the Casson parameter have the consequences seen in Figure 11, which show that a larger Casson parameter results in a smaller trapped bolus. The Helmholtz-Smoluchowski parameter exhibits unusual behavior, as shown in Figure 12. When this value is increased, the bolus becomes smaller. The influence of the thermophoresis parameter is shown to reduce the size of the trapped bolus (see Figure. 13). Finally, the Brownian motion parameter is shown to have the opposite impact in Figure 14, making the trapped bolus within the fluid flow more substantial.

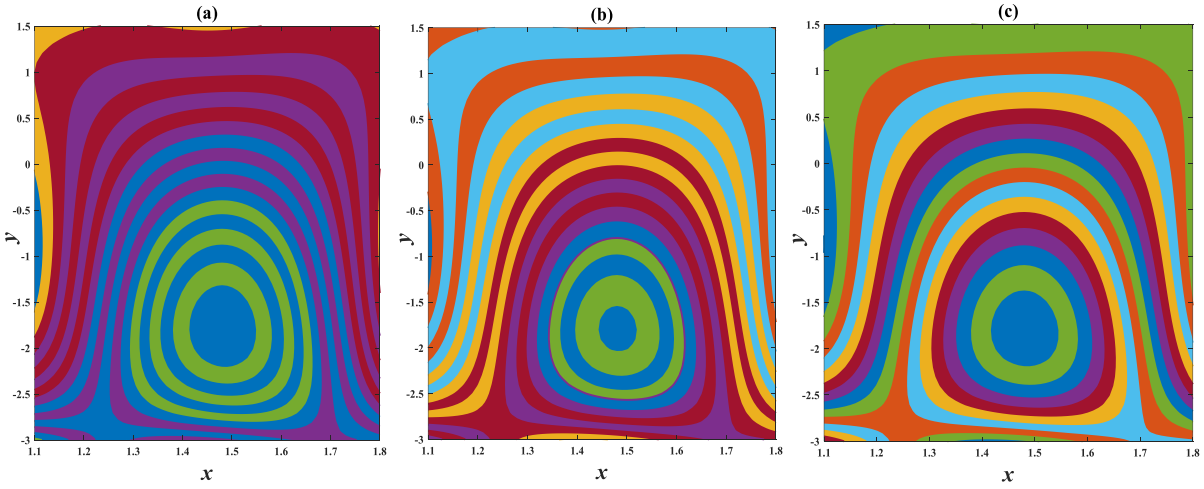

Fig. 10. Streamlines via*Mn*

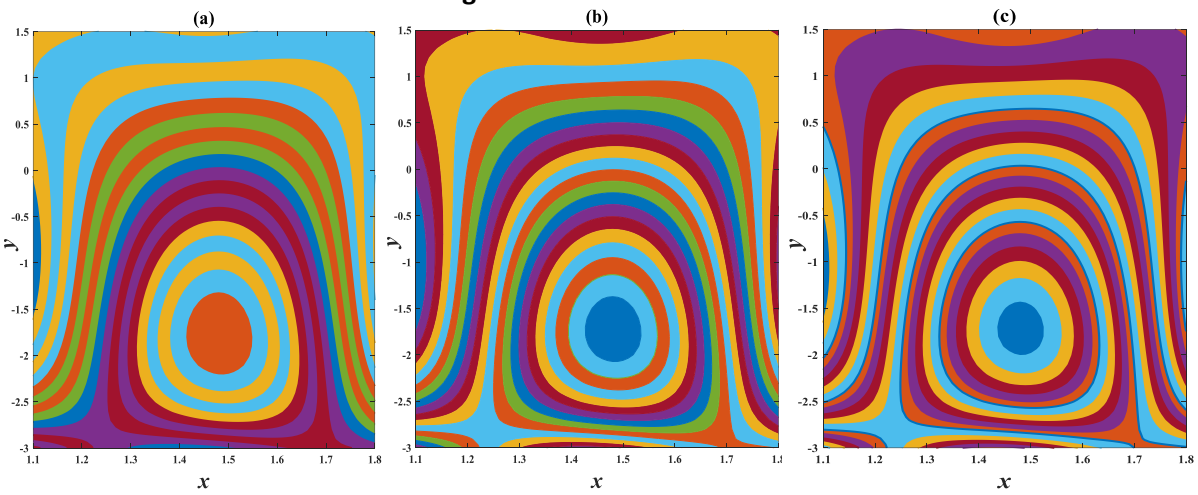

Fig. 11. Streamlines via *β*

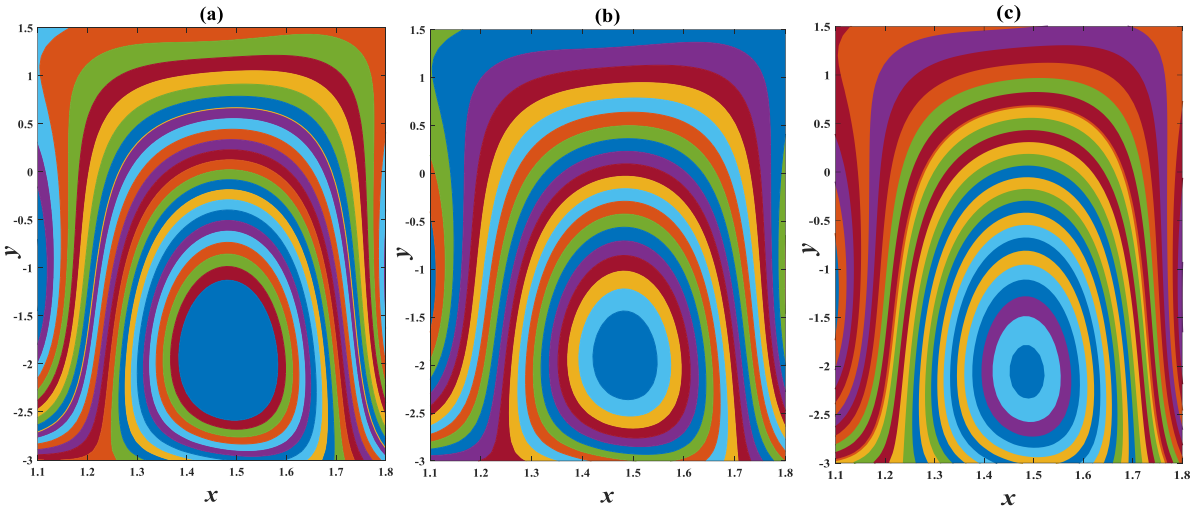

Fig. 12. Streamlines via U_{hs}

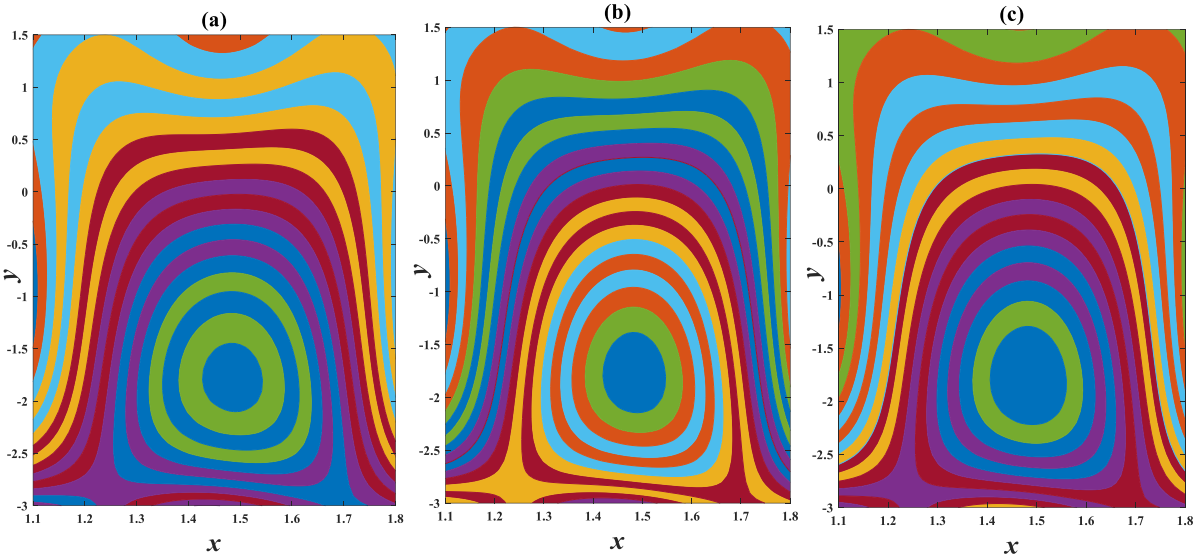

Figure. 13. Streamlines via *Nt*

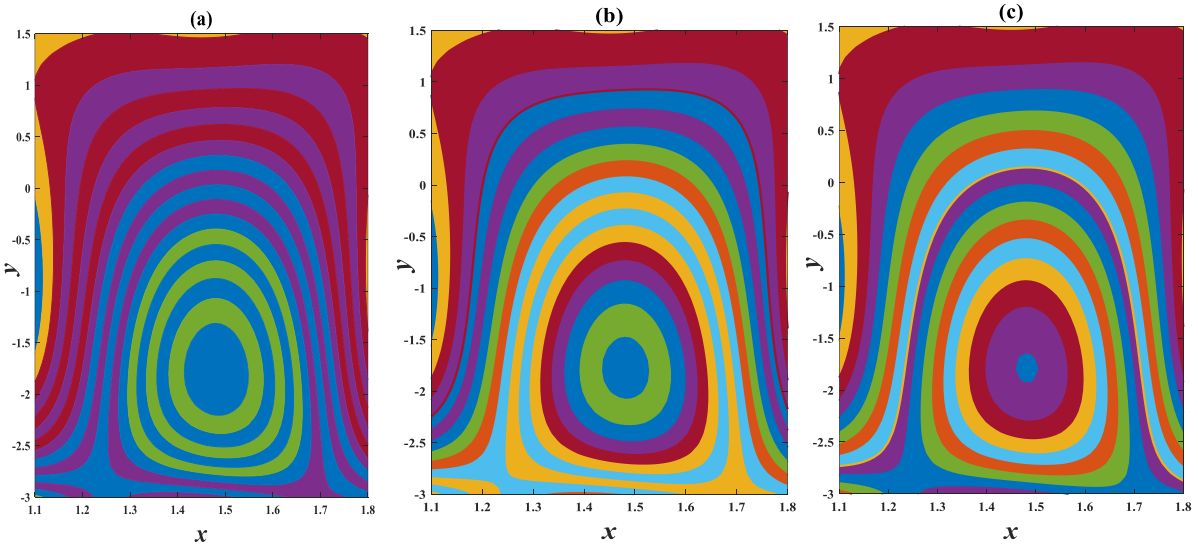

Fig. 14. Streamlines via *Nb*

5. Final Interpretations

Since magnetic effects and convective circumstances are important in MHD (Magnetohydrodynamics) peristaltic mechanism of Casson nanofluids within a vertical non-uniform conduit, we have undertaken a thorough investigation on the impact of electroosmotic generation in this context. This study goes into the impact of several factors that can majorly affect physiological variables. Understanding complex processes, like blood flow through micro-arteries, is a top priority, and this research represents a major step in that direction. The results of this study can also inform the design of future medical equipment such as roller-finger pumps, heart-lung machines, and dialysis machines. Some of our most important findings are as follows:

i. When comparing Newtonian and Casson fluids, we find that the former have greater velocities and temperatures while the latter have more significant concentrations.
ii. Increased fluid concentration is caused by a magnetic field, which significantly affects both velocity and temperature. This may have ramifications for the application of magnetic fields to cancer treatment.
iii. It has been found that the non-uniform parameter increases as a function of temperature.
iv. The shear stress of non-Newtonian nanofluids is greater than that of their parent non-Newtonian fluids.
v. The Nusselt number varies as a function of the magnetic effect parameter; when this value is decreased, the Nusselt number decreases.
vi. As the thermophoresis parameter goes down, the Sherwood number goes up.
vii. The pressure increase for the mean flow significantly lowers non-uniformity term values.
viii. When the Casson term is included, the trapped bolus grows as the fluid flows around it.

These results contribute to basic and applied research in medicine and engineering by shedding light on the complex dynamics of the peristalsis of nanofluid under the impact of many circumstances.

References:

[1] Choi, S. US, and Jeffrey A. Eastman. *Enhancing thermal conductivity of fluids with nanoparticles*. No. ANL/MSD/CP-84938; CONF-951135-29. Argonne National Lab.(ANL), Argonne, IL (United States), 1995.
[2] Buongiorno, Jacopo. "Convective transport in nanofluids." (2006): 240-250. https://doi.org/10.1115/1.2150834
[3] Alawi, O. A., NA Che Sidik, S. N. Kazi, and M. Kh Abdolbaqi. "Comparative study on heat transfer enhancement and nanofluids flow over backward and forward facing steps." *Journal of Advanced Research in Fluid Mechanics and Thermal Sciences* 23, no. 1 (2016): 25-49.
[4] Nadeem, S., and Hina Sadaf. "Exploration of single wall carbon nanotubes for the peristaltic motion in a curved channel with variable viscosity." *Journal of the Brazilian Society of Mechanical Sciences and Engineering* 39 (2017): 117-125. https://doi.org/10.1007/s40430-016-0612-9
[5] Aman, Sidra, Syazwani Mohd Zokri, Zulkhibri Ismail, Mohd Zuki Salleh, and Ilyas Khan. "Effect of MHD and porosity on exact solutions and flow of a hybrid Casson-nanofluid." *Journal of Advanced Research in Fluid Mechanics and Thermal Sciences* 44, no. 1 (2018): 131-139.
[6] Hayat, T., Farhat Bibi, S. Farooq, and A. A. Khan. "Nonlinear radiative peristaltic flow of Jeffrey nanofluid with activation energy and modified Darcy's law." *Journal of the Brazilian Society of Mechanical Sciences and Engineering* 41 (2019): 1-11. https://doi.org/10.1007/s40430-019-1771-2
[7] Bosli, Fazillah, Alia Syafiqa Suhaimi, Siti Shuhada Ishak, Mohd Rijal Ilias, Amirah Hazwani Abdul Rahim, and Anis Mardiana Ahmad. "Investigation of nanoparticles shape effects on aligned MHD casson nanofluid flow and heat transfer with convective boundary condition." *Journal of Advanced Research in Fluid Mechanics and Thermal Sciences* 91, no. 1 (2022): 155-171. https://doi.org/10.37934/arfmts.91.1.155171
[8] Srinivas, A. N. S., C. Haseena, and S. Sreenadh. "Peristaltic transport of nanofluid in a vertical porous stratum with heat transfer effects." *BioNanoScience* 9 (2019): 117-130. https://doi.org/10.1007/s12668-018-0571-y
[9] Gbadeyan, J. A., E. O. Titiloye, and A. T. Adeosun. "Effect of variable thermal conductivity and viscosity on Casson

nanofluid flow with convective heating and velocity slip." *Heliyon* 6, no. 1 (2020). https://doi.org/10.1016/j.heliyon.2019.e03076

[10] Abo-Dahab, S. M., M. A. Abdelhafez, Fateh Mebarek-Oudina, and S. M. Bilal. "MHD Casson nanofluid flow over nonlinearly heated porous medium in presence of extending surface effect with suction/injection." *Indian Journal of Physics* 95, no. 12 (2021): 2703-2717. https://doi.org/10.1007/s12648-020-01923-z

[11] Latham, Thomas Walker. "Fluid motions in a peristaltic pump." PhD diss., Massachusetts Institute of Technology, 1966.

[12] Vaidya, Hanumesh, C. Rajashekhar, G. Manjunatha, and K. V. Prasad. "Peristaltic mechanism of a Rabinowitsch fluid in an inclined channel with complaint wall and variable liquid properties." *Journal of the Brazilian Society of Mechanical Sciences and Engineering* 41 (2019): 1-14. https://doi.org/10.1007/s40430-018-1543-4

[13] Manjunatha, G., C. Rajashekhar, Hanumesh Vaidya, K. V. Prasad, and K. Vajravelu. "Impact of heat and mass transfer on the peristaltic mechanism of Jeffery fluid in a non-uniform porous channel with variable viscosity and thermal conductivity." *Journal of Thermal Analysis and Calorimetry* 139, no. 2 (2020): 1213-1228. https://doi.org/10.1007/s10973-019-08527-8

[14] Manjunatha, G., C. Rajashekhar, Hanumesh Vaidya, K. V. Prasad, O. D. Makinde, and J. U. Viharika. "Impact of variable transport properties and slip effects on MHD Jeffrey fluid flow through channel." *Arabian Journal for Science and Engineering* 45 (2020): 417-428. https://doi.org/10.1007/s13369-019-04266-y

[15] Rajashekhar, C., F. Mebarek-Oudina, Hanumesh Vaidya, K. V. Prasad, G. Manjunatha, and H. Balachandra. "Mass and heat transport impact on the peristaltic flow of a Ree–Eyring liquid through variable properties for hemodynamic flow." *Heat Transfer* 50, no. 5 (2021): 5106-5122. https://doi.org/10.1002/htj.22117

[16] Akbar, Noreen Sher, S. Nadeem, T. Hayat, and Awatif A. Hendi. "Peristaltic flow of a nanofluid with slip effects." *Meccanica* 47 (2012): 1283-1294. https://doi.org/10.1007/s11012-011-9512-3

[17] Mustafa, M., S. Hina, T. Hayat, and A. Alsaedi. "Influence of wall properties on the peristaltic flow of a nanofluid: analytic and numerical solutions." *International Journal of Heat and Mass Transfer* 55, no. 17-18 (2012): 4871-4877. https://doi.org/10.1016/j.ijheatmasstransfer.2012.04.060

[18] Akbar, Noreen Sher, S. Nadeem, Changhoon Lee, Zafar Hayat Khan, and Rizwan Ul Haq. "Numerical study of Williamson nano fluid flow in an asymmetric channel." *Results in Physics* 3 (2013): 161-166.

[19] Kothandapani, M., and J. Prakash. "Effect of radiation and magnetic field on peristaltic transport of nanofluids through a porous space in a tapered asymmetric channel." *Journal of Magnetism and Magnetic Materials* 378 (2015): 152-163. https://doi.org/10.1016/j.jmmm.2014.11.031

[20] Sreenadh, S., E. Sudhakara, M. Krishnamurthy, and G. Gopi Krishna. "MHD convection flow of a couple stress fluid through a vertical porous stratum." *World Applied Sciences Journal* 33, no. 6 (2015): 918-930.

[21] Abbasi, F. M., T. Hayat, and A. Alsaedi. "Peristaltic transport of magneto-nanoparticles submerged in water: model for drug delivery system." *Physica E: Low-dimensional Systems and Nanostructures* 68 (2015): 123-132. https://doi.org/10.1016/j.physe.2014.12.026

[22] Kothandapani, M., and J. Prakash. "Effects of thermal radiation parameter and magnetic field on the peristaltic motion of Williamson nanofluids in a tapered asymmetric channel." *International Journal of Heat and Mass Transfer* 81 (2015): 234-245. https://doi.org/10.1016/j.ijheatmasstransfer.2014.09.062

[23] Ahmed, B. I. L. A. L., T. A. R. I. Q. Javed, and M. U. H. A. M. M. A. D. Sajid. "Peristaltic transport of blood in terms of Casson fluid model through a tube under impact of magnetic field for moderate Reynolds number." *Imaging Science Journal* 14 (2018): 101-113.

[24] Javed, T., B. Ahmed, A. H. Hamid, and M. Sajid. "Numerical analysis of peristaltic transport of Casson fluid for non-zero Reynolds number in presence of the magnetic field." *Nonlinear Engineering* 7, no. 3 (2018): 183-193. https://doi.org/10.1515/nleng-2017-0098

[25] Javid, Khurram, Nasir Ali, and Zeeshan Asghar. "Rheological and magnetic effects on a fluid flow in a curved channel with different peristaltic wave profiles." *Journal of the Brazilian Society of Mechanical Sciences and Engineering* 41, no. 11 (2019): 483. https://doi.org/10.1007/s40430-019-1993-3

[26] Warke, A. S., K. Ramesh, F. Mebarek-Oudina, and A. Abidi. "Numerical investigation of the stagnation point flow of radiative magnetomicropolar liquid past a heated porous stretching sheet." *Journal of Thermal Analysis and Calorimetry* (2022): 1-12. https://doi.org/10.1007/s10973-021-10976-z

[27] Vaidya, Hanumesh, Kerehalli Vinayaka Prasad, Rajashekhar Choudhari, Shivaraya Keriyappa, Manjunatha Gudekote, and Jyoti Shetty. "Partial slip effects on MHD peristaltic flow of Carreau-Yasuda fluid (CY) through a planner micro-channel." *Journal of Advanced Research in Fluid Mechanics and Thermal Sciences* 104, no. 2 (2023): 65-85.

[28] Sanil, Prathiksha, Manjunatha Gudekote, Rajashekhar Choudhari, Hanumesh Vaidya, and Kerehalli Vinayaka Prasad. "Heat Transfer Analysis on Peristaltic Transport of Sisko Fluid in an Inclined Uniform Channel." *Journal of Advanced Research in Fluid Mechanics and Thermal Sciences* 103, no. 2 (2023): 157-179.

https://doi.org/10.37934/arfmts.103.2.157179
[29] Ahmed, Bilal, Asma Ashraf, and Fizza Anwar. "Inertial considerations in peristaltically activated MHD blood flow model in an asymmetric channel using Galerkin finite element simulation for moderate Reynolds number." *Alexandria Engineering Journal* 75 (2023): 495-512. https://doi.org/10.1016/j.aej.2023.05.088
[30] Ijaz, N., Ahmed Zeeshan, and S. U. Rehman. "Effect of electro-osmosis and mixed convection on nano-bio-fluid with non-spherical particles in a curved channel." *Mechanics & Industry* 19, no. 1 (2018): 108. https://doi.org/10.1051/meca/2017040
[31] Tripathi, Dharmendra, Ashish Sharma, and O. Anwar Bég. "Joule heating and buoyancy effects in electro-osmotic peristaltic transport of aqueous nanofluids through a microchannel with complex wave propagation." *Advanced Powder Technology* 29, no. 3 (2018): 639-653. https://doi.org/10.1016/j.apt.2017.12.009
[32] Hussain, Sadaqut, Nasir Ali, and Kaleem Ullah. "Peristaltic flow of Phan-Thien-Tanner fluid: effects of peripheral layer and electro-osmotic force." *Rheologica Acta* 58 (2019): 603-618. https://doi.org/10.1007/s00397-019-01158-8
[33] Asgari, Alitaghi, Quyen Nguyen, Arash Karimipour, Quang-Vu Bach, Maboud Hekmatifar, and Roozbeh Sabetvand. "Develop molecular dynamics method to simulate the flow and thermal domains of H 2 O/Cu nanofluid in a nanochannel affected by an external electric field." *International Journal of Thermophysics* 41 (2020): 1-14. https://doi.org/10.1007/s10765-020-02708-6
[34] Waheed, S., S. Noreen, D. Tripathi, and D. C. Lu. "Electrothermal transport of third-order fluids regulated by peristaltic pumping." *Journal of Biological Physics* 46 (2020): 45-65. https://doi.org/10.1007/s10867-020-09540-x
[35] Choudhari, Rajashekhar, Hanumesh Vaidya, Fateh Mebarek-Oudina, Abderrahim Wakif, Manjunatha Gudekote, Kerehalli Vinayaka Prasad, Kuppalapalle Vajravelu, and Shivaraya Keriyapa. "Electro-kinetically modulated peristaltic mechanism of jeffrey liquid through a micro-channel with variable viscosity." *Thermal Science* 25, no. Spec. issue 2 (2021): 271-277. https://doi.org/10.2298/TSCI21S2271C
[36] Tanveer, Anum, Sidra Mahmood, Tasawar Hayat, and Ahmed Alsaedi. "On electroosmosis in peristaltic activity of MHD non-Newtonian fluid." *Alexandria Engineering Journal* 60, no. 3 (2021): 3369-3377. https://doi.org/10.1016/j.aej.2020.12.051
[37] Rafiq, Maimona, Mehmoona Sajid, Sharifa E. Alhazmi, M. Ijaz Khan, and Essam Rashdy El-Zahar. "MHD electroosmotic peristaltic flow of Jeffrey nanofluid with slip conditions and chemical reaction." *Alexandria Engineering Journal* 61, no. 12 (2022): 9977-9992. https://doi.org/10.1016/j.aej.2022.03.035
[38] Abbasi, A., A. Zaman, W. Farooq, and M. F. Nadeem. "Electro-osmosis modulated peristaltic flow of oldroyd 4-constant fluid in a non-uniform channel." *Indian Journal of Physics* (2021): 1-13. https://doi.org/10.1007/s12648-020-02002-z
[39] Vaidya, Hanumesh, Rajashekhar Choudhari, Dumitru Baleanu, K. V. Prasad, Shivaleela, M. Ijaz Khan, Kamel Guedri, Mohammed Jameel, and Ahmed M. Galal. "On electro-osmosis in peristaltic blood flow of magnetohydrodynamics carreau material with slip and variable material characteristics." *International Journal of Modern Physics B* 37, no. 04 (2023): 2350032. https://doi.org/10.1142/S0217979223500327